SAND2000-8471J

Short-range order types in binary alloys: A reflection of coherent phase stability

C. Wolverton

Ford Research Laboratory, MD3028/SRL, Dearborn, MI 48121-2053

V. Ozoliņš

Sandia National Laboratories, Livermore, CA 94551

Alex Zunger

National Renewable Energy Laboratory, Golden, CO 80401

(October 27, 1999)

Abstract

The short-range order (SRO) present in disordered solid solutions is classified according to three characteristic system-dependent energies: (1) formation enthalpies of ordered compounds, (2) enthalpies of mixing of disordered alloys, and (3) the energy of coherent phase separation, (the composition-weighted energy of the constituents each constrained to maintain a common lattice constant along an A/B interface). These energies are all compared against a common reference, the energy of incoherent phase separation (the composition-weighted energy of the constituents each at their own equilibrium volumes). Unlike long-range order (LRO), short-range order is determined by energetic competition between phases *at a fixed composition*, and hence only *coherent* phase-separated states are of relevance for SRO. We find five distinct SRO types, and show examples of each of these five types, including Cu-Au, Al-Mg, GaP-InP, Ni-Au, and Cu-Ag. The SRO is calculated from

DISCLAIMER

Short-range order types in binary alloys: A reflection of coherent phase stability

C. Wolverton

Ford Research Laboratory, MD3028/SRL, Dearborn, MI 48121-2053

V. Ozoliņš

Sandia National Laboratories, Livermore, CA 94551

Alex Zunger

National Renewable Energy Laboratory, Golden, CO 80401

(October 27, 1999)

Abstract

The short-range order (SRO) present in disordered solid solutions is classified according to three characteristic system-dependent energies: (1) formation enthalpies of ordered compounds, (2) enthalpies of mixing of disordered alloys, and (3) the energy of coherent phase separation, (the composition-weighted energy of the constituents each constrained to maintain a common lattice constant along an A/B interface). These energies are all compared against a common reference, the energy of incoherent phase separation (the composition-weighted energy of the constituents each at their own equilibrium volumes). Unlike long-range order (LRO), short-range order is determined by energetic competition between phases *at a fixed composition*, and hence only *coherent* phase-separated states are of relevance for SRO. We find five distinct SRO types, and show examples of each of these five types, including Cu-Au, Al-Mg, GaP-InP, Ni-Au, and Cu-Ag. The SRO is calculated from

first-principles using the mixed-space cluster expansion approach combined with Monte Carlo simulations. Additionally, we examine the effect of inclusion of coherency strain in the calculation of SRO, and specifically examine the appropriate functional form for accurate SRO calculations.

I. INTRODUCTION: SHORT-RANGE ORDER AND COHERENT PHASE STABILITY

The equilibrium regions involved in solid-state binary alloy phase diagrams are ordered phases, two-phase regions, and disordered solid solutions. The latter form at elevated temperatures, and consist of an $A_{1-x}B_x$ phase in which the A and B atoms of the alloy are distributed in a disordered fashion on the sites of a single, underlying lattice (often a Bravais lattice, e.g., fcc). In the disordered phase, the atomic-scale occupation of sites of the lattice by A and$B$ atoms does not occur perfectly randomly, nor does it occur with any long-range atomic ordering. Instead, local ordering or local clustering takes place in this solid solution, and is collectively referred to as short-range order (SRO). The degree and type of SRO in a solid solution can be quantified by specifying the Warren-Cowley SRO parameters, α_{lmn} for a given composition (x) and temperature (T):

$$\alpha_{lmn}(x,T) = 1 - \frac{P_{lmn}^{A(B)}(x,T)}{x}. \tag{1}$$

Here, $P_{lmn}^{A(B)}(x,T)$ is the conditional probability that given an A atom at the origin, there is a B atom at shell (lmn). This probability is necessarily dependent on composition and temperature, thus giving an $x-$ and $T-$dependence to α. If the lattice sites are occupied completely at random, the conditional probability $P(x,T)$ is equal to x, and thus α=0. Therefore, the departure of α from zero indicates the extent to which *atom-atom correlations* exist within disordered alloys. Ordering-type correlations (the predominance of $A-B$ bonds) manifest themselves as $\alpha < 0$ while clustering-type correlations (the predominance of $A-A$ and $B-B$ bonds) manifest themselves as $\alpha > 0$.

In diffraction experiments, short-range order does not give rise to superstructure reflections (as in the case of long-range order), and hence one must look "under" or "between" the Bragg diffraction peaks to observe SRO. The SRO gives rise to modulations in the monotonic Laue background, and using diffuse scattering techniques, (e.g., see Refs. [1–7]) one can examine these modulations between the Bragg peaks. By analyzing the diffuse scattered

intensity, one can extract the portion, $I^{\rm SRO}_{\rm diffuse}$, of the diffuse scattering due to SRO, which is proportional to the lattice Fourier transform of the Warren-Cowley parameters:

$$I^{\rm SRO}_{\rm diffuse} \propto \alpha(x,\mathbf{k}) = \sum_{lmn}^{n_R} \alpha_{lmn}(x) e^{i\mathbf{k}\cdot\mathbf{R}_{lmn}}. \quad (2)$$

The connection between high-temperature SRO in the disordered phase and the low-temperature structures is fascinating. [3,8,9] As one cools the disordered phase, it eventually gives way to long-range order (LRO), either in the form of ordered compounds or phase-separation. Are the SRO fluctuations of the high-temperature disordered phase simply "precursors" or "remnants" of the underlying LRO in the low-temperature phase, or can there be a competition between local ordering/clustering *vs.* long-range ordering/clustering? This question can be phrased more quantitatively as follows: The maximum of Eq. (2) indicates the dominant wavevector $\mathbf{k}_0^{\rm SRO}$ for SRO fluctuations in the disordered phase. Long-range order at low-T is often similarly characterized by an ordered structure composed of a dominant composition wave, $\mathbf{k}_0^{\rm LRO}$. [10,11] The question is then: What is the relationship between $\mathbf{k}_0^{\rm SRO}$ and $\mathbf{k}_0^{\rm LRO}$? Although in many cases, $\mathbf{k}_0^{\rm SRO} = \mathbf{k}_0^{\rm LRO}$, there are many examples [3,8,9] where the dominant wavevector of SRO and LRO do not coincide. [12] Some of these cases of distinct wavevectors can be explained [8] by noting that whereas SRO is determined by the energetic competition between all possible phases *at a fixed composition*, LRO stability is determined by the energy relative to all possible mixtures of phases, *even those at different compositions*.

II. QUALITATIVE UNDERSTANDING OF LRO *VS.* SRO

To understand the distinction between fixed-composition and global stability, and the concomitant differences between SRO and LRO, we define three characteristic energies:

(a) The formation enthalpy of an ordered (O) structure is the total energy $E_O(\sigma, a_\sigma)$ of the ordered phase σ with lattice constant a_σ, taken with respect to equivalent amounts of the A and B constituents, each at their "natural", equilibrium lattice constants a_A and a_B, respectively

$$\Delta H_O = E_O(\sigma, a_\sigma) - [(1-x)E_A(a_A) + xE_B(a_B)]. \tag{3}$$

(b) The mixing enthalpy of a random (R) alloy is the analogous energy difference for the random alloy:

$$\Delta H_R = E_R(R, a_\sigma) - [(1-x)E_A(a_A) + xE_B(a_B)] \tag{4}$$

Notice that in both Eqs. (3) and (4) the reference energies are A at its lattice constant a_A and B at a_B. For alloys with lattice mismatched constituents ($a_A \neq a_B$), incoherent mixtures of phases with different volumes often contain misfit dislocations at the interfaces between the two phases to relieve strain. Thus, the reference energies of Eqs. (3) and (4) involve a state of phase separation (A+B) which is incoherent. Thus, we define the incoherent phase separated (IPS) state as

$$E_{\rm IPS} = [(1-x)E_A(a_A) + xE_B(a_B)] \tag{5}$$

and is simply chosen as the zero reference energy for our comparisons. In contrast, *coherent* two-phase mixtures contain no such misfit dislocations, and thus both phases are somewhat strained due to this constraint of coherency. This leads to:

(c) The Coherent Phase Separated State or coherency strain (CS), which involves strain in the plane of the interface and relaxation of the atoms perpendicular to the interface. Thus, the strain energy necessary to maintain coherency at an interface between A and B (called the "coherency strain") is necessarily dependent on the orientation of the interface $\mathbf{k}$. $\Delta E_{\rm CS}(\hat{k}, x)$, the coherency strain energy, is defined as the energy change when the bulk solids A and B are deformed from their equilibrium cubic lattice constants a_A and a_B to a common lattice constant $a_\perp$ in the direction perpendicular to $\hat{k}$, while they are relaxed in the direction parallel to $\hat{k}$: [13]

$$\Delta E_{\rm CS}(\hat{k}, x) = \min_{a_\perp} \left[(1-x)\Delta E_A^{\rm epi}(\hat{k}, a_\perp) + x\Delta E_B^{\rm epi}(\hat{k}, a_\perp)\right] \tag{6}$$

where $\Delta E_A^{\rm epi}(\hat{k}, a_\perp)$ is the energy required to deform A biaxially to $a_\perp$. Each of the energies $\Delta E_A^{\rm epi}$ and $\Delta E_B^{\rm epi}$ are positive definite, and hence, the coherency strain of Eq. (6) is positive definite. Of particular importance is the lowest attainable coherency strain

$$\Delta E_{\rm CS}^{\rm min}(x) = \min_{\hat{k}} \Delta E_{\rm CS}(\hat{k}, x) \tag{7}$$

where the minimization is performed over all directions $\hat{k}$. $\Delta E_{\rm CS}^{\rm min}(x)$ then gives the formation enthalpy of the energetically most favorable coherently phase-separated state.

Using the definitions of Eqs. (3)-(6), we can now note that:

(1) *Long-range order is determined by incoherent phase stability*: for a *long-range ordered* compound to be a ground state (a zero-temperature stable phase), it must be lower in energy than any other compound at that composition, as well as lower in energy than any *incoherent* two-phase mixture of phases at other compositions, including a mixture of the constituent elements. Thus, a necessary condition for a ground state structure is that $\Delta H_O < 0$. The formation energy ΔH_O of Eq. (3) demonstrates clearly that the long-range order, and hence the equilibrium phase diagram behavior is determined by incoherent phase stability.

(2) *Short-range order is determined by coherent phase stability*: The short-range order involves a single-phase field (disordered solid solution) of the phase diagram, and thus does not pertain to incoherent two-phase mixtures. [12] In fact, two crucial quantities towards determining the types of fluctuations which develop in disordered alloys are the "ordering energy"

$$\delta E_{\rm ord} = \Delta H_O - \Delta H_R \tag{8}$$

and the "coherent phase-separation energy"

$$\delta E_{\rm CPS} = \Delta E_{\rm CS}^{\rm min} - \Delta H_R \tag{9}$$

$\delta E_{\rm ord}$ ($\delta E_{\rm CPS}$) represent the energy required to form the ordered (coherent phase-separated) state, starting from the random alloy of the same composition. Both $\delta E_{\rm ord}$ and $\delta E_{\rm CPS}$ are fixed-composition energy differences and are independent of the energy of incoherent phase separation.

Figure 1 illustrates five possible relative orders of the energies ΔH_O, ΔH_R, and $\Delta E_{\rm CS}$ of Eqs. (3)-(6). The ordered structures "O" in Fig. 1 are representative of the lowest-energy coherent configurations, i.e., structures with dominant composition waves at the Brillouin

zone boundary (e.g., the $L1_0$, $L1_1$, or $L1_2$ structures). It should be noted that in cases (e.g., Al-Cu) where the lowest-energy coherent configurations correspond to ordered compounds which have a large degree of "clustering", one can obtain clustering-type SRO even in a "Type I" alloy (see Ref. [14]). In this paper, we study these types I-V of LRO/SRO behavior in real alloy systems using a first-principles total energy technique for calculating ΔH_O and $\Delta E_{\rm CS}$, and a cluster expansion method for calculating ΔH_R and SRO.

The salient features of the SRO are decided by the quantities $\delta E_{\rm ord}$ and $\delta E_{\rm CPS}$, so we examine the qualitative possibilities for these two quantities, defining the five alloy types of Fig. 1:

Type I: $\delta E_{\rm ord} < 0 < \delta E_{\rm CPS}$ (e.g., Cu-Au)

Type II: $\delta E_{\rm ord} < 0 \sim \delta E_{\rm CPS}$ (e.g., Al-Mg)

Type III: $\delta E_{\rm ord} < \delta E_{\rm CPS} < 0$ (e.g., GaP-InP)

Type IV: $\delta E_{\rm ord} \sim \delta E_{\rm CPS} < 0$ (e.g., Ni-Au)

Type V: $\delta E_{\rm CPS} < \delta E_{\rm ord} < 0$ (e.g., Cu-Ag)

The arrows in Fig. 1 show schematically the fluctuations in the random alloy which are energetically most favorable. In "Type I", "Type II", and "Type III" alloys, the ordered alloy is lower in energy than both the random alloy ($\delta E_{\rm ord} < 0$) and the coherent phase separated state ($\delta E_{\rm ord} < \delta E_{\rm CPS}$). Therefore, energetic fluctuations of the random alloy are expected to be be of ordering type, depicted as $R \rightarrow O$ in Fig. 1. Thus, the SRO of solid solutions of Types I, II, and III alloys are all ordering type ($\mathbf{k}_{\rm SRO} \neq 0$), even though the LRO is ordering only in Types I and II, but phase-separating (incoherently) in Type III. On the other hand, a "Type V" alloy is a prototypical "clustering" alloy, where the coherent phase separated state is lower in energy than both the random alloy ($\delta E_{\rm CPS} < 0$) and the ordered alloy ($\delta E_{\rm CPS} < \delta E_{\rm ord}$). Hence, the SRO is expected to be of clustering-type ($\mathbf{k}_{\rm SRO} = 0$), represented by $R \rightarrow CS$ in Fig. 1. Since phase separation is the lowest-energy incoherent state in a "Type V" alloy, the LRO of this alloy is also phase separation. "Type IV" alloys, are intermediate between "Type III" and "Type V". In type IV, there is strong competition between ordering and coherent phase separation ($\delta E_{\rm ord} \sim \delta E_{\rm CPS}$), and thus, it is difficult to

predict even the qualitative behavior of the SRO for this case, since there are expected to be competitive energetic fluctuations simultaneously towards ordering and phase separation in these alloys (illustrated by both $R \rightarrow O$ and $R \rightarrow CS$ arrows in Fig. 1). As shown below, the SRO of the "Type IV" alloy, Ni-Au, is intermediate between a strongly ordering alloy (Types I, II, and III) and a strongly clustering alloy (Type V).

III. THE MIXED-SPACE CLUSTER EXPANSION - A DESCRIPTION OF ATOMICALLY-RELAXED, COHERENT ALLOY ENERGETICS

A. General Formalism

Calculating the equilibrium SRO in solid solutions from an energetic approach requires, in principle, a statistical sampling of all configurations σ. Even a binary alloy system with a modest number of sites N possesses 2^N possible configurations, and hence the number of configurations for which we need to know the energy quickly becomes impractically large. Hence, one method used to obtain finite-T thermodynamics is to perform statistical calculations by means of a Monte Carlo algorithm using an energy functional which describes the alloy in question. The Monte Carlo calculations efficiently sample the energy in regions of configuration space where the energy is close to its thermal average. Still, Monte Carlo calculations require the alloy energy functional be sufficiently computationally inexpensive so that it is easily evaluated for very large unit cells and for many different configurations. Hence, we wish to use a method whereby one maps first-principles alloy energetics onto an energy functional which is sufficiently simple so that Monte Carlo simulations become possible, but also sufficiently accurate to reflect the atomically-relaxed energetics of a wide variety of alloy configurations. Such a method, the mixed-space cluster expansion (CE), has been developed [15,16] and applied to several alloy systems. [17–21] The CE method relies on (i) a separation of formation enthalpy into strain and chemical contributions, and (ii) a mapping of the chemical term onto a generalized Ising-like model: One selects a single,

underlying parent lattice (in the case of this paper, fcc) and defines a configuration, σ, by specifying the occupations of each of the N lattice sites by an A-atom or a B-atom. For each configuration, one assigns the spin-occupation variables, $\hat{S}_i = \pm 1$ to each of the N sites. Within the Ising-like description of the mixed-space CE, the positional degrees of freedom are integrated out, leaving an energy functional of spin variables only $\hat{S}_i$ which reproduces for each configuration σ the energy of the *atomically relaxed structure*, with atomic positions at their equilibrium (zero-force, zero-stress) values.

The details of construction of this energy functional within the LDA are discussed elsewhere, [15,20] and thus we give here only the salient points. We have used full-potential, fully-relaxed, linearized augmented plane wave method [22] (LAPW) total energies in the construction of the mixed-space cluster expansions. (In the case of GaP-InP, LAPW energies were used to fit a ternary valence-force-field functional, which was in turn used to construct the mixed-space cluster expansion. [23]) Details of the LAPW method typically used in these calculations, as well as the number and types of alloy structures used in the CE fit are described in Ref. [20].

The expression used for the formation energy (the energy with respect the the compositional average of the alloy constituents) of any configuration σ in the mixed-space CE is

$$\Delta H(\sigma) = \sum_{\mathbf{k}} J(\mathbf{k}) |S(\mathbf{k},\sigma)|^2 + \sum_f D_f \, J_f \, \overline{\Pi}_f(\sigma) + \frac{1}{4x(1-x)} \sum_{\mathbf{k}} \Delta E_{\rm CS}(\hat{k},x) |S(\mathbf{k},\sigma)|^2. \quad (10)$$

$J(\mathbf{k})$ is the Fourier transform of the pair interaction energies, $S(\mathbf{k},\sigma)$ is the structure factor for σ, f is a symmetry-distinct figure comprised of several lattice sites (pairs, triplets, etc.), D_f is the number of figures per lattice site, J_f is the Ising-like interaction for the figure f, and the "lattice-averaged product" $\overline{\Pi}_f$ is defined as a product of the variables $\hat{S}_i$, over all sites of the figure f with the overbar denoting an average over all symmetry equivalent figures of lattice sites. Our approach is based on the fact that for simple configurations σ we know the left-hand side of Eq. (10) quite accurately from first-principles LDA total energies,

so we can solve for the interaction energies $\{J_f\}$ and $J(\mathbf{k})$. Thus, we incorporate at the outset, a detailed quantum mechanical picture (LDA) for interactions, and hence for SRO. Also, we note that the total energy includes eigenvalue (or one-electron), electrostatic, and exchange-correlation terms.

The mixed-space CE of Eq. (10) is separated into three parts:

(i) The first summation includes *all pair figures* corresponding to pair interactions with arbitrary separation. These pair interactions are conveniently summed using the reciprocal-space concentration-wave formalism. [10,11] $J(\mathbf{k})$ and $S(\mathbf{k},\sigma)$ are the lattice Fourier transforms of the real-space pair interactions and spin-occupation variables, J_{ij} and $\hat{S}_i$, respectively.

(ii) The second summation includes only *non-pair figures*. The real-space summation of Eq. (10) is over f, the symmetry-distinct non-pair figures (points, triplets, etc.).

(iii) The third summation involves $\Delta E_{\rm CS}(\hat{k},x)$, the *coherency strain energy*, defined above.

B. The Attenuated Coherency Strain Term

The reason to include a $\Delta E_{\rm CS}$ term in Eq. (10) is to describe the elastic strain effects between lattice-mismatched phases brought into contact and strained as a result of coherency. To understand the need for this term in the cluster expansion, consider a subset of coherent two-phase configurations: Long period $n \to \infty$ superlattices A_n/B_n with layer orientation along $\hat{k}$. These long-period structures possess small ($\mathbf{k} \to 0$) dominant wavevectors, but their strain energy depends on the layer orientation, thus the *direction* of $\mathbf{k}$, as seen in Eq. (6). However, the cluster expansion of Eq. (10) *without* $\Delta E_{\rm CS}$ and with finite-ranged interactions will give [24] $\Delta H(n) \sim 1/n$ as $n \to \infty$, independent of $\hat{k}$. Thus, one must include a $\Delta E_{\rm CS}$ term in Eq. (10) since this introduces the orientation dependence in coherently-strained two-phase configurations, which cannot be described by short-ranged real-space interactions $J(R)$. Further, because long-period superlattices possess $\mathbf{k} \to 0$ dominant wavevectors, but

the strain energy is dependent on the direction of $\hat{k}$, there is a $\mathbf{k} \to 0$ non-analyticity in the reciprocal-space description of the coherency strain. Thus, the coherency strain cannot be described everywhere by reciprocal-space interactions $J(\mathbf{k})$ which are analytic.

Laks *et al.* [15] formulated $\Delta E_{\rm CS}$ by insuring that it retained the correct $n \to \infty$ superlattice limit:

$$\Delta E_{\rm CS}(\sigma) = \frac{1}{4x(1-x)} \sum_{\mathbf{k}} \Delta E_{\rm CS}(\hat{k}, x) |S(\mathbf{k}, \sigma)|^2 \tag{11}$$

Laks *et al.* demonstrated that this form gives the correct orientation- and composition-dependence in the long-period limit of the coherency strain. [15] Furthermore, it was shown that this form is uniquely defined for short-period superlattices and non-superlattices. However, this form treats short-period superlattices ($\mathbf{k} \to 2\pi/n$) the same way that long-period superlattices ($\mathbf{k} \to \infty$) are treated. To generalize Eq. (11), we note that the $\mathbf{k} \to 0$ non-analyticity could still be satisfied if we were to multiply $E_{\rm CS}$ by a function $F(\mathbf{k})$:

$$\Delta E_{\rm CS}(\sigma) = \frac{1}{4x(1-x)} \sum_{\mathbf{k}} \Delta E_{\rm CS}(\hat{k}, x) |S(\mathbf{k}, \sigma)|^2 F(\mathbf{k}) \tag{12}$$

so long as $F(\mathbf{k}) \to 1$ as $\mathbf{k} \to 0$ for all directions. However, the introduction of $F(\mathbf{k})$ enables different treatments of short- *vs.* long-period systems. So, the question is: Which $F(k)$ is best?

We exploit the inherent flexibility in the choice of the form of $F(\mathbf{k})$ to improve the convergence of the cluster expansion. Intuitively, one might expect that $\Delta E_{\rm CS}$ of Eq. (12) should be related to the strain energy inherent in the structure, and thus related to the relaxation energy

$$\delta E_{\rm rel} = E_{\rm LDA}^{\rm relaxed} - E_{\rm LDA}^{\rm unrelaxed}. \tag{13}$$

Indeed, consider the following decomposition of the formation enthalpy of any configuration σ (either ordered or random):

$$\Delta H(\sigma) = \Delta E_{\rm VD}(\sigma) + \delta E_{\rm chem}^{\rm UR}(\sigma) + \delta E_{\rm rel}(\sigma) \tag{14}$$

The first term on the right-hand side is the "volume deformation energy", i.e., the energy required to deform the alloy constituents hydrostatically from their equilibrium lattice constants to that of the alloy structure σ. The second term is the "chemical energy", i.e., the energy difference between the unrelaxed (UR) structure (with all atoms at iead lattice sites) and $\Delta E_{\rm VD}$, so that $\Delta E_{\rm VD} + \delta E^{\rm UR}_{\rm chem} = \delta E^{\rm UR}_{\rm LDA}$. The third term, the "relaxation energy", is the energy gained upon atomic and cell-shape distortions.

In systems where $\delta E_{\rm rel}$ is small, the CE is rapidly convergent. [20] However, large relaxations lead to long-ranged pair and multibody interactions. For an A_mB_n long-period superlattice,

$$\delta E_{\rm rel}(A_mB_n, \hat{k}) = \Delta E_{\rm CS}(\hat{k}, x) - \Delta E_{\rm VD}(x) \tag{15}$$

Substituting Eq. (15) into Eq. (14), we find that

$$\Delta H(A_mB_n, \hat{k}) = \Delta E_{\rm CS}(\hat{k}, x) + \Delta E^{\rm UR}_{\rm chem} \tag{16}$$

in accordance with Eq. (10). Eq. (15) holds for infinte superlattices only, but we want a form which gives a reasonable relaxation energy for short-period ordered structures and disordered alloys as well, i.e., we want to introduce a wavevector-dependence into Eq. (15). Within a second-order expansion of the elastic energy, $\delta E_{\rm rel}$ can be written as [10,11]

$$\delta E_{\rm rel}(\sigma) = -\sum_{\mathbf{k}} V_{\rm rel}(\mathbf{k}) |S(\mathbf{k}, \sigma)|^2 \tag{17}$$

where $V_{\rm rel}(\mathbf{k})$ can be related to the lattice Fourier transforms of the Kanzaki forces and dynamical matrix. [10,11] We will retain the form of Eq. (17), but we will generalize $V_{\rm rel}(\mathbf{k})$ to accomodate some of the shortcomings of the second-order expansion derivation.

To gain insight into the wavevector-dependence of the relaxation energy, consider the following breakdown of the relaxation energy:

$$\delta E_{\rm rel}(\sigma) = \delta E^{\rm int}_{\rm rel}(\sigma) + \delta E^{\rm ext}_{\rm rel}(\sigma) \tag{18}$$

The cell-internal relaxation $\delta E^{\rm int}_{\rm rel}$ is the energy gained when atomic positions within the unit cell are relaxed, but the unit-cell vectors maintain their ideal angles and lengths, whereas

the cell-external relaxation $\delta E_{\rm rel}^{\rm ext}$ is the energy gained when the unit-cell vectors are allowed to relax. For some high-symmetry structures, $\delta E_{\rm rel}^{\rm int} = 0$ by symmetry: Structures with dominant composition wavevectors at the Brillouin zone boundary often possess only cell-external degrees of freedom. For example, the A_1B_1 superlattice along (001) is tetragonal, composed of $\mathbf{k} = (001)$ waves, and possesses only the tetragonality ratio c/a as a symmetry-allowed degree of freedom. However, the A_2B_2 (001) superlattice is composed of $\mathbf{k} = \frac{1}{2}(001)$ waves, and in addition to the c/a ratio, also possess a cell-internal degree of freedom.

It is interesting to know the extent to which cell-internal and cell-external relaxations are energetically important in various alloy systems. Table I shows the LAPW calculated relaxation energy for A_2B_2 and A_1B_1 (001) superlattice structures for a variety of size-mismatched noble-metal and aluminum-alloy systems: Ni-Au, Cu-Au, Cu-Ag, Ni-Al, Cu-Al, and Al-Mg. The relaxation energy is decomposed into cell-internal and cell-external pieces. Table I demonstrates that (i) when symmetry does not prohibit cell-*internal* relaxation, this mode of relaxation is dominant (e.g., 100% in Al_2Mg_2). Yet, (ii) cell-*external* relaxation is not negligible: It is 100% (by symmetry) for A_1B_1 along (001) or (111); it is ~50% for (001) Cu_2Al_2, and ~10-15% for Ni_2Au_2 and Cu_2Au_2. (iii) The A_2B_2 structure has much larger (mostly cell-internal) relaxation than the A_1B_1 structure. Similar studies [15] on longer-period A_nB_n superlattices confirm that $\delta E_{\rm rel}$ increases with n. *Thus, the cell-internal relaxation decays as the dominant wavevector* $\mathbf{k} \sim 1/n$ *increases towards the Brillouin zone boundary* (small period superlattices). However, cell-external relaxation does not. In the second-order expansion approaches, it can be shown [10] that the relaxation energy decays precisely to zero at the Brillouin zone boundary. Thus, these types of approaches do not account for energy lowering due to cell-*external* relaxations. For some systems (Al-Mg), this is probably an adequate assumption, while for others (Ni-Al, Cu-Al) it is not. It is possible to introduce macroscopic elastic strain into the first-principles linear response approaches, [25] however, to our knowledge this approach has not been applied to studies of bulk alloy systems. In this vein, we also note that linear response and alchemical calculations have been extended to third order. [26,27] However, to our knowledge, none of these third-order

approaches treats the effects of macroscopic elastic strain, required to describe cell-external relaxations. To obtain a non-zero relaxation energy at the Brillouin zone boundary, $V_{\rm rel}(\mathbf{k})$ will be given by

$$\tilde{V}_{\rm rel}(k) = \frac{\Delta E_{VD}(x) - \Delta E_{CS}(x,\hat{\mathbf{k}})}{4x(1-x)} F(\mathbf{k}) \tag{19}$$

where $F(\mathbf{k})$ is chosen so that the relaxation energy from Eq. (19) matches the first-principles values obtained from Eq. (13). We have selected [28]

$$F(\mathbf{k}) = e^{-(|\mathbf{k}|/k_c)^2} \tag{20}$$

with k_c being an adjustable parameter. We find that

$$\delta E_{\rm rel}(\sigma) = -\frac{1}{2}\sum_{\mathbf{k}} \frac{\Delta E_{VD}(x) - \Delta E_{CS}(x,\hat{\mathbf{k}})}{4x(1-x)} |S(\sigma,\mathbf{k})|^2 e^{-(|\mathbf{k}|/k_c)^2} \tag{21}$$

with $k_c \sim 0.6(2\pi/a_0)$ matches the LDA relaxation energies (e.g., Table I) of many compounds very well, hence we will use

$$\Delta E_{\rm CS}(\sigma) = \frac{1}{4x(1-x)} \sum_{\mathbf{k}} \Delta E_{\rm CS}(\hat{k},x) |S(\mathbf{k},\sigma)|^2 e^{-(|\mathbf{k}|/k_c)^2} \tag{22}$$

in our cluster expansion instead of Eq. (11) of $E_{CS}(\sigma)$. The resulting mixed-space cluster expansion then is

$$\begin{aligned} \Delta H(\sigma) = &\sum_{\mathbf{k}} J(\mathbf{k}) |S(\mathbf{k},\sigma)|^2 + \sum_f D_f\, J_f\, \overline{\Pi}_f(\sigma) \\ &+ \frac{1}{4x(1-x)} \sum_{\mathbf{k}} \Delta E_{\rm CS}(\hat{k},x) |S(\mathbf{k},\sigma)|^2 e^{-(|\mathbf{k}|/k_c)^2} \end{aligned} \tag{23}$$

We refer to Eq. (22) as the "attenuated coherency strain". It differs from previous calculations in the choice of $F(\mathbf{k})$ of Eq. (20) rather than $F(\mathbf{k}) = 1$.

To summarize this section, we find that Eq. (23) improves the conventional cluster expansion since the effect of strain for large-k (small-period) structures is attenuated. This will turn out to be important when *anharmonic strain is large* and when the relaxation energy of short-period, $\mathbf{k} \to \frac{\pi}{n}$ structures is particularly small relative to that of long-period $\mathbf{k} \to 0$ structures, so treating them equally [as is the case if $F(\mathbf{k}) = 1$] is unbalanced. Since

attenuation does not affect $\mathbf{k} \rightarrow 0$ energetics, it is unimportant for phase-separating systems where the SRO peaks near $\mathbf{k}$=0.

We next discuss the $F(\mathbf{k}) = 1$ form of the coherency strain energy [Eq. (11)] used in the mixed-space CE of Eq. (23) and show how it can fail for some short-period superlattices in systems which possess strongly anharmonic strain. The failures include prediction of spurious ground state structures, and incorrect short-range order patterns (when compared with measured patterns). Attenuating the form of the coherency strain energy via Eq. (20) is shown to rectify these problems.

C. Attenuating the coherency strain for short-period superlattices

The problems which can arise with the unattenuated form of the CS are most easily explained with an example: Cu-rich Cu-Au alloys. This system has a very large lattice constant mismatch (12%), and thus anharmonic strain effects are significant. First-principles calculations of the coherency strain in Cu-Au alloys [20] have shown that the strong anharmonic strain of Au results in a low CS for the (201) direction in Cu-rich alloys. This simply means that (201) long-period superlattices (small $\mathbf{k}$) will be lower in energy than differently-oriented long-period superlattices. However, this energetic preference for (201) structures does not necessarily hold for short-period superlattices (large $\mathbf{k}$), due to the first two terms of Eq. (10) which describe interfacial energies of atoms near the Cu/Au interfaces. But the unattenuated form of the coherency strain energy given in Eq. (11) will give a large energy lowering to *any* Cu-rich structure which possesses composition waves lying along the (210) direction, regardless of the *magnitude* of the wave (the superlattice period). Thus, the short-period Cu_4Au_1 superlattice along (210), which is a structure composed of composition waves at the origin and $\mathbf{k} = 2/5(210)$ (a rather large $\mathbf{k}$, 80% of the way to the Brillouin zone boundary) will be given a low energy by Eq. (11) due to the low energy of the small-$\mathbf{k}$ long-period (210) superlattices. [29] This is illustrated in Fig. 2 which shows the unattenuated ($F = 1$) and attenuated cluster expansion predictions for the formation

enthalpy of this Cu_4Au_1 structure as well as the directly-calculated LAPW formation enthalpy. The SRO of $Cu_{0.9}Au_{0.1}$ is shown in Fig. 3 as calculated by the unattenuated and attenuated CE, as well as obtained from diffuse scattering measurements. [30] The $F = 1$ unattenuated CE has the following features: (1) The Cu_4Au_1 (210) superlattice is artificially low in energy due to the low (210) CS energy (Fig. 2). (2) The $F = 1$ cluster expansion incorrectly predicts this structure's energy to lie below the tie-line connecting Cu_3Au ($L1_2$) and Cu, in disagreement with both experiment and direct LAPW calculations. (3) As we see from Fig. 3, the unattenuated $F = 1$ cluster expansion predicts (210)-type SRO in the solid solution for Cu-rich alloys. The predicted SRO along the (210) direction is due to the low (210) long-period superlattice energy for Cu-rich alloys. However, the measured SRO pattern [30] shows peaks at the (100) points.

The effects of attenuating the CS are significant: (1) The form of $F(\mathbf{k})$ of Eq. (20) progressively attenuates the CS for structures with larger wavevectors. Thus, in our example, the energy of the *short*-period Cu_4Au_1 superlattice is not given an artifically large relaxation energy due to the large relaxation energy of the *long*-period (210) superlattices. Consequently, its energy is raised significantly, in excellent agreement with direct LAPW calculations (Fig. 2), despite this fact that this energy was not used in fitting either the attenuated or unattenuated CE. (2) The energy of Cu_4Au_1 is brought above the tie-line connecting Cu_3Au + Cu; thus, attenuating the CS solves the problem of false ground states due to low energy long-period strain energies. (3) Fig. 3 shows that the SRO pattern is brought into quantitative agreement with experiment by the attenuation. Calculated peaks in the SRO move from the (210) direction to the (100) direction upon attenuation of the CS. Thus, we see that the form of the attenuated coherency strain is most likely to be crucial in ordering systems (where wavevectors away from the origin are important) which possess highly anharmonic strain energies (where the soft elastic direction can shift as a function of composition).

Next, we discuss the short-range order behavior for a series of alloys classified according to their energetics as in Figure 1. We show that the Al-Mg system represents a Type II

alloy, which has not previously been discussed. We specifically point to the strong effect of attenuating the CS for the Cu-Au and Ni-Au systems, and show that the attenuated strain leads to SRO in Cu-rich Cu-Au alloys in agreement with experiment and significantly changes the predicted SRO in Ni-rich Ni-Au, for which there are currently no measurements.

IV. SHORT-RANGE ORDER TYPES

We now investigate the SRO/LRO types of Fig. 1. The calculations of some of these alloy systems (Cu-Au, Ni-Au, and Cu-Ag) have been discussed previously [17] using the unattenuated $F = 1$ form of the coherency strain. Thus, for these alloys, we do not provide a detailed account of the experimental and theoretical literature on the SRO of these solid solutions. Rather, we discuss the effects of attenuating the coherency strain on the SRO, and compare with experimental diffuse scattering measurements where appropriate.

A. Type I alloy, Cu-Au: $\delta E_{\rm ord} < 0 < \delta E_{\rm CPS}$

Cu-Au is the prototypical ordering alloy system. Its compounds exhibit negative formation and mixing enthalpies, $\Delta H_O < 0$, $\Delta H_R < 0$ (see Ref. [20] for a recent compilation of the mixing and formation enthalpies in this system). The ordering energies are negative, $\delta E_{\rm ord} < 0$ as is the coherent phase separation energy $\delta E_{\rm CPS} < 0$, placing this alloy into "Type I" of Fig. 1. [31] Figure 3 shows the calculated SRO $\alpha(\mathbf{k})$ for $Cu_{0.9}Au_{0.1}$. The SRO of this system has recently been measured [30] by diffuse x-ray scattering, and the measured results are also shown in Fig. 3 for comparison. As expected for a "Type I" alloy, the SRO shows ordering type fluctuations (peaks in the SRO off the Γ point) consistent with the $R \rightarrow O$ arrow schematically illustrated in Fig. 1. The calculated SRO pattern with attenuated SRO is in quantitative agreement with the measured results [30], which also shows (100)-type SRO.

B. Type II alloy, Al-Mg: $\delta E_{\rm ord} < 0 \sim \delta E_{\rm CPS}$

The Al-Mg phase diagram shows a series of complex ordered compounds. Calculations of ordered Al-Mg compounds show [32,33] that the low-energy fcc-based compounds have a negative formation enthalpy, $\Delta H_O < 0$, whereas the mixing enthalpy of the solid solution phase is positive, $\Delta H_R > 0$, both from experiment [34] and theory. [33] First-principles calculations of the heat of solution of Mg impurities in Al also show a positive formation enthalpy. [35] Thus, the ordering energy is negative, and because the coherency strain energy is comparable to the mixing energy $\delta E_{\rm CPS} \sim 0$, and thus Al-Mg is a Type II alloy. The calculated SRO of an $Al_{0.85}Mg_{0.15}$ solid solution is shown in Fig. 4. Table I shows that the cell-external relaxation energy of ordered Al-Mg compounds is nearly zero and that the relaxation is almost completely due to cell-internal relaxations. But, for structures with wavevectors near the Brillouin zone boundary such as an Al_1Mg_1 (001) superlattice, there are no cell-internal degrees of freedom, and thus the total relaxation energy is nearly zero (despite the fact that this cell is tetragonal). Hence, the relaxation tendencies in this system follow the attenuated form of Eq. (20), and thus we have performed the calculations for this system using the attenuated CS. The calculated SRO shows a clear ordering tendency with peaks at $\langle 100 \rangle$, despite the fact that $\Delta H_R > 0$. These (100) fluctuations in the solid solution are interesting since aged Al-Mg alloys show the existence of an ordered Al_3Mg ($L1_2$) phase in the precipitation sequence, [36,33] with this structure being composed of (100) composition waves. The metastable $L1_2$ phase does not appear in the Al-Mg phase diagram because the equilibrium phases are incoherent with the fcc Al matrix; however, based on the existence of $L1_2$ in coherent precipitation experiments, one might expect that the metastable coherent phase diagram contains this phase. Thus, the (100)-type fluctuations in the SRO are a reflection of the underlying coherent phase stability of the (100)-type Al_3Mg phase. Note that the calculated SRO fluctuations follow the $R \rightarrow O$ schematic of Fig. 1. To our knowledge, there have been no measurements (diffuse scattering or otherwise) of the SRO in Al-Mg solid solutions.

C. Type III alloy, GaP-InP: $\delta E_{\rm ord} < \delta E_{\rm CPS} < 0$

The GaP-InP alloy system possesses positive formation enthalpies for all bulk structures, $\Delta H_O > 0, \Delta H_R > 0$, but a negative ordering energy, $\delta E_{\rm ord} < 0$. [8,18,23] In other words, the formation enthalpy of low-energy ordered compounds is below that of the random alloy ($\delta E_{\rm ord} < 0$) as is the coherency strain energy ($\delta E_{\rm CPS} < 0$). (Surface ordering [37,24] is another effect whereby $\Delta H_O^{\rm bulk} > 0$ in bulk but the constraint of coherent epitaxy (epi) changes the sign of $\Delta H_O^{\rm epi} < 0$ near the surface.) Further, Lu *et al.* [18] have shown that the SRO in this system is ordering, thus making it a Type III alloy. Another previous study [38] suggests that Ti-V might be a Type III alloy. Figure 5 shows the SRO calculated for $Ga_{0.5}In_{0.5}P$ using the cluster expansion of Ref. [23]. The calculations of Fig. 5 were obtained from a cluster expansion constructed from a "ternary" valence force field model which was carefully fit to a large database of LAPW formation enthalpies. [23] In contrast, the cluster expansion of Ref. [18] was directly fit to LAPW energetics, with no force field as an intermediate step. Other than the GaP-InP cluster expansion used in Fig. 5, all other cluster expansions in this paper were constructed directly from first-principles total energies. The SRO of $Ga_{0.5}In_{0.5}P$ clearly shows an ordering tendency, with peaks at the $(1\frac{1}{2}0)$ positions, as found by Lu *et al.* [18] The lowest-energy coherent ordered structures in the GaP-InP system correspond to (210)-type short-period superlattices, as these structures possess the optimal geometry for relaxation of tetrahedrally-coordinated systems. The calculated SRO is a manifestation of these low-energy (210) structures, and corresponds to the $R \rightarrow O$ fluctuations, schematically illustrated in Fig. 1 for "Type III" alloys.

D. Type IV alloy, Ni-Au: $\delta E_{\rm ord} \sim \delta E_{\rm CPS} < 0$

Ni-Au alloys show positive formation enthalpies $\Delta H_O > 0$, positive mixing enthalpies $\Delta H_R > 0$, a miscibility gap in the phase diagram, and yet both measurements [4] and calculations [8,17,39] of the SRO of $Ni_{0.4}Au_{0.6}$ show peaks off the Γ point, just like GaP-InP.

However, in contrast with GaP-InP, the CS energy in Ni-Au is slightly lower than the lowest-energy ordered phase. Thus, as illustrated in Fig. 1, there will be energetically favorable fluctuations in the random alloy towards both ordering ($R \rightarrow O$) and coherent phase separation ($R \rightarrow CS$). The competition between these two types of fluctuations distinguishes "Type IV" Ni-Au from "Type III" GaP-InP. In GaP-InP, only $R \rightarrow O$ fluctuations are energetically favorable, as the CS energy is much higher in energy than the lowest-energy ordered phase.

Using an unattenuated form for the CS, we previously [17] calculated the SRO of Ni-Au alloys for the $Ni_{0.4}Au_{0.6}$ composition (where we could compare with experiment) as well as for other compositions where there are currently no measurements. Like the Cu-Au system, the CS energy of Ni-Au shows strong anharmonic effects, and the soft elastic direction for Ni-rich alloys is (210) due to the elastic response of Au under compression. Thus, just as in Fig. 3 for Cu-Au, we found the unattenuated SRO calculation for Ni-rich Ni-Au alloys produced SRO peaks along the $(\langle \xi \frac{\xi}{2} 0 \rangle)$ direction. Because we have found this SRO to be incorrect for the Cu-Au alloys, we also want to re-examine the SRO for Ni-rich (and Au-rich alloys) and evaluate the effects of attenuating the CS for these alloys. Figure 6 shows the calculated SRO for $Ni_{0.75}Au_{0.25}$ both for unattenuated and attenuated CS. The SRO peaks change position when the more correct, attenuated form of the CS is used. The SRO shows peaks along the $(\xi 00)$ line, in accordance with the measured (and calculated) SRO peaks for $Ni_{0.40}Au_{0.60}$. Thus, the SRO in Fig. 6 with attenuated CS is a more accurate prediction of the SRO for *Ni-rich* Ni-Au alloys than our previous calculations. [17] However, the previous calculations of the SRO in *Au-rich* $Ni_{0.40}Au_{0.60}$ were in qualitative agreement with experiment. Thus, it is important to see that attenuating the CS does not change the SRO peak position for Au-rich alloys. Figure 7 shows the calculated SRO for $Ni_{0.40}Au_{0.60}$. Clearly, for Au-rich alloys, the attenuation of the CS does not affect the SRO in a qualitative way, and leaves the calculated SRO in agreement with diffuse scattering measurements. [4]

E. Type V alloy, Cu-Ag: $\delta E_{\rm CPS} < \delta E_{\rm ord} < 0$

Cu-Ag is a prototypical "phase-separating" alloy, which exhibits positive formation enthalpies $\Delta H_O > 0$, positive mixing enthalpies $\Delta H_R > 0$, a miscibility gap, and the coherent phase-separated state is *lower* in energy than both the random alloy and ordered compounds. This latter fact distinguishes Cu-Ag from GaP-InP and Ni-Au. In GaP-InP, the CS energy is above that of ordered compounds, and in Ni-Au the CS energy is slightly below, but very close in energy to that of ordered compounds. The calculations of SRO in Cu-Ag have been discussed previously and the SRO was shown to be clustering (with peaks at Γ). [17] In Fig. 8 we show the SRO for a $Cu_{0.95}Ag_{0.05}$ alloy at T=480K. Although this is a different composition and temperature than the calculations of Ref. [17], the SRO still shows clustering-type peaks at (000). The effect of attenuating the CS is not likely to have a significant effect since the attenuation does not affect the energetics near the Γ point, where the SRO shows peaks. Thus, for clustering alloys, the attenuated CS is likely to be unimportant.

V. SUMMARY

Short-range order reflects an energetic competition between perfectly random and imperfectly random alloys *at the same composition.* In contrast, long-range order reflects not only this iso-compositional competition, but also an energetic competition between a compound at composition x, and its constituents at compositions $x = 0$ and $x = 1$ (and, more generally, between two-phase mixtures of compounds at any compositions). This simple picture enables us to divide SRO *vs.* LRO behavior of alloys into five generic groups:

(i) *Type I (most compound-forming systems, e.g., Cu-Au)*, where $\Delta H_O < 0$ (i.e., ordering type LRO) and where $\Delta H_O < \Delta H_R$ so the random alloy can lower its energy by developing ordering-type SRO (Fig. 3). Thus, the dominant wavevectors $\mathbf{k}_{\rm LRO}$ and $\mathbf{k}_{\rm SRO}$ are both ordering type ($\mathbf{k} \neq 0$).

(ii) *Type II (e.g., Al-Mg)*, where $\Delta H_O < 0$ (i.e., ordering type LRO) but $\Delta H_R > 0$

(unstable random alloy). Here too, the random alloy can lower its energy by developing ordering-type SRO patterns, even though $\Delta H_R > 0$ (Fig. 4). Again, both $\mathbf{k}_{\text{LRO}}$ and $\mathbf{k}_{\text{SRO}}$ are ordering-type.

(iii) *Type III (e.g., most semiconductor alloys and perhaps Ti-V)*, where $\Delta H_O > 0$ (i.e., phase-separating LRO) and $\Delta H_R > 0$ (unstable random alloy), but $\Delta H_O < \Delta H_R$. Here, the random alloy can lower its energy by adopting ordering-type SRO ($\mathbf{k}_{\text{SRO}} \neq 0$) even though the LRO is phase-separating $\mathbf{k}_{\text{LRO}} = 0$. Thus, $\mathbf{k}_{\text{LRO}} \neq \mathbf{k}_{\text{SRO}}$.

(iv) *Type IV (e.g., Ni-Au)*, where $\Delta H_O > 0$ (i.e., phase-separating LRO) and $\Delta H_R > 0$ (i.e., unstable random alloy), but $\Delta H_O < \Delta H_R$ (as in Type III) *and* $\Delta E_{CS} < \Delta H_R$. Here, the random alloy can lower its energy in *two* channels: by developing fluctuations akin to the ordered phase ($\mathbf{k}_{\text{SRO}} \neq 0$) or fluctuations corresponding to phase-separation ($\mathbf{k}_{\text{SRO}} = 0$).

(v) *Type V (most phase-separating materials, e.g., Cu-Ag)*, where $\Delta H_O > 0$ (i.e., phase-separating LRO), $\Delta H_R > 0$ (unstable random alloy) *and* $\Delta E_{CS} << \Delta H_O$. Here, the random alloy can lower its energy only by developing phase-separating fluctuations, so both $\mathbf{k}_{\text{LRO}}$ and $\mathbf{k}_{\text{SRO}}$ are clustering-type.

This classification scheme (Fig. 1) enables one to guess the qualitative SRO behavior of an alloy given the measured or calculated enthalpies of ordered and random systems. It introduces three unusual cases (Types II, III, and IV), in addition to the usual ordering (Type I) and phase-separating (Type V) cases. By noting that SRO reflects a constant-composition energy balance between two phases, one recognizes the possibilities of having ordering SRO coexisting with phase-separating LRO (Type III).

To accurately calculate the short-range order profile we utilize the first-principles mixed-bases cluster expansion [Eq. (10)], where the coherency strain energy is first separated out from the total energy, and the remainder ("chemical energy") which reflects the constant composition term is expanded in (a momentum-space series of) pair interactions and in (a real-space series of) many-body interactions. We found here that in those alloy systems where the long-period structures (corresponding to $\mathbf{k} \rightarrow 0$) have very different relaxation energies for some ordering directions than the short-period structures (corresponding to

$\mathbf{k} \to \frac{\pi}{n}$), a wavevector-dependent term $F(|\mathbf{k}|)$ must be introduced into the coherency strain to produce a balanced description. Examples include structures with very large size mismatch such as Cu-Au and Ni-Au, where anharmonic effects lead to large relaxation energies for a particular ordering direction in long-period structures, while short-period structures do not have such a large relaxation. $F(|\mathbf{k}|)$ then attenuates the $\mathbf{k} \to \frac{\pi}{n}$ relaxation energy with respect to that of $\mathbf{k} \to 0$. For phase-separating systems, where the SRO occurs near $\mathbf{k} = 0$, the function $F(|\mathbf{k}|)$ makes no change. Similarly, at the compositions where anharmonic effects are weak (Au-rich Ni-Au or Cu-Au), the $F(|\mathbf{k}|)$ function makes no changes even for size-mismatched alloys. We find that this new, attenuated form of the coherency srain, when combined with our first-principles cluster expansion, produces SRO patterns in excellent agreement with diffuse-scattering experiments.

V. O. gratefully acknowledges support from the Office of Energy Research (OER) [Division of Materials Science of the Office of Basic Energy Sciences (BES)], U. S. Department of Energy, under contract No. DE-AC04-94-AL85000. Work performed at the National Renewable Energy Laboratory was supported by the Office of Energy Research (OER) [Division of Materials Science of the Office of Basic Energy Sciences (BES)], U. S. Department of Energy, under contract No. DE-AC36-98-GO10337.

REFERENCES

[1] L. H. Schwartz and J. B. Cohen, *Diffraction from Materials*, Academic Press, New York, 1977.

[2] S. C. Moss, in *Local Atomic Arrangements Studied by X-ray Diffraction*, edited by J. B. Cohen and J. E. Hilliard, pp. 95-122. New York: Gordon and Breach (1966).

[3] F. Solal, R. Caudron, F. Ducastelle, A. Finel, and A. Loiseau, Phys. Rev. Lett. **58**, 2245 (1987).

[4] T. B. Wu and J. B. Cohen, Acta Metall. **31**, 1929 (1983).

[5] L. Reinhard, B. Schönfeld, G. Kostorz, and W. Bührer, Phys. Rev. B **44**, 1727 (1990).

[6] L. Reinhard, J. L. Robertson, S. C. Moss, G. E. Ice, P. Zschack, and C. J. Sparks, Phys. Rev. B **45**, 2662 (1992).

[7] J. E. Epperson, J. P. Anderson, and H. Chen, Metall. and Mat. Trans. **25A**, 17 (1994).

[8] Z. W. Lu and A. Zunger, Phys. Rev. B **50**, 6626 (1994).

[9] C. Wolverton and A. Zunger, Phys. Rev. B **52**, 8813 (1995).

[10] D. de Fontaine, Solid State Phys. **34** 73 (1979).

[11] A. G. Khachaturyan, *Theory of Structural Transformations in Solids* (Wiley, New York, 1983).

[12] We note that the distinction between coherent and incoherent phase stability only accounts for *some* of the cases for which long- and short-range order do not coincide. Other cases illustrating the distinction between long-range order and short-range order have been found, [3,9] where contributions to the free energy such as configurational entropy or electron-hole free energy can differentiate energetics at low temperature (LRO) and at high temperature (SRO).

[13] In the general case of a low-symmetry (e.g., high Miller index) interface, there are three independent plane strain components instead of just the uniform plane strain described by $a_\perp$ (see ref. [24]). Eq. (6) is exact for interfaces possessing high symmetry axes, such as (100) and (111) in fcc-based systems.

[14] S. Müller, C. Wolverton, L.-W. Wang, and A. Zunger, Phys. Rev. B (in press, 1999).

[15] D. B. Laks, L. G. Ferreira, S. Froyen, and A. Zunger, Phys. Rev. B **46**, 12587 (1992).

[16] A. Zunger, in *NATO ASI on Statics and Dynamics of Alloy Phase Transformations,* (Plenum Press, New York, 1994), p. 361.

[17] C. Wolverton, V. Ozoliņš, and A. Zunger, Phys. Rev. B **57**, 4332 (1998).

[18] Z. -W. Lu, D. B. Laks, S. -H. Wei, and A. Zunger, Phys. Rev. B **50**, 6642 (1994).

[19] C. Wolverton and A. Zunger, Phys. Rev. Lett. **75**, 3162 (1995).

[20] V. Ozoliņš, C. Wolverton, and A. Zunger, Phys. Rev. B **57**, 6427 (1998).

[21] C. Wolverton, Phil. Mag. Lett. **79**, 683 (1999).

[22] S. -H. Wei and H. Krakauer, Phys. Rev. Lett. **55**, 1200 (1985); D. J. Singh, *Planewaves, Pseudopotentials, and the LAPW Method*, (Kluwer, Boston, 1994).

[23] C. Wolverton and A. Zunger, Phys. Rev. Lett. **75**, 3162 (1995).

[24] V. Ozoliņš, C. Wolverton and A. Zunger, Phys. Rev. B **57**, 4816 (1998).

[25] M. Peressi and S. Baroni Phys. Rev. B **49**, 7490 (1994).

[26] A. Debernardi and S. Baroni, Solid State Commun. **91**, 813 (1994); A. Debernardi, S. Baroni, and E. Molinari, Phys. Rev. Lett. **75**, 1819 (1995).

[27] K. Leung and E. Stechel (unpublished).

[28] L. G. Ferreira, V. Ozolins, and A. Zunger, Phys. Rev. B **60**, 1687 (1999).

[29] It is important to note that the anharmonic CS is *correct* near the origin of reciprocal space, or for long-period Cu/Au superlattices (i.e., within LDA, 201 is really the softest elastic direction for highly distorted Au); The use of the soft 201 direction for wavevectors away from the origin is where the problems of the unattenuated CE arise.

[30] B. Schoenfeld, M. J. Portmann, S. Y. Yu, and G. Kostorz, Acta Mater. **47**, 1413 (1999).

[31] We have classified Cu-Au as "Type I" according to Fig. 1. However, it should be noted that the mixing energy of the completely random alloy in Cu-Au is nearly zero; only when the energetic effect of SRO is included does the mixing energy of the disordered solid solution become negative (see Ref. [20]).

[32] S. Narasimhan and J. W. Davenport, Phys. Rev. B **51**, 659 (1995).

[33] C. Wolverton (unpublished).

[34] J. A. Brown and J. N. Pratt, Metall. Trans. **1**, 2743 (1970); Y. Zuo and Y. A. Chang, CALPHAD **17**, 161 (1993); D. Ludecke and K. Hack, Z. Metallkd. **77**, 145 (1986).

[35] N. Chetty, M. Weinert, T. S. Rahman, and J. W. Davenport, Phys. Rev. B **52**, 6313 (1995).

[36] T. Sato, Y. Kojima, and T. Takahashi, Met. Trans. **13A**, 1373 (1982); K. Osamura and T. Ogura, Met. Trans. **15A**, 835 (1984).

[37] A. Zunger and S. Mahajan, in *Handbook of Semiconductors*, 2nd ed., edited by S. Mahajan (Elsevier, Amsterdam, 1988), p. 133.

[38] L. Reinhard and P. E. A. Turchi, Phys. Rev. Lett. **72**, 120 (1994).

[39] M. Asta and S. M. Foiles, Phys. Rev. B **53**, 2389 (1996).

TABLES

TABLE I. LAPW calculated relaxation energies [Eq. (13)] in a variety of noble metal- and aluminum-alloys. Shown are the relaxation energies for A_2B_2 (001) and A_1B_1 (001) superlattices. The former possesses both cell-internal and cell-external degrees of freedom; and the latter possesses only a cell-external degree of freedom. The fraction of the relaxation energy which comes from the cell-internal relaxation is shown, and to give some idea of the scale of the relaxation energy, the ratio between the relaxation energy and the formation enthalpy of the structure is also given.

A_2B_2 (001) Superlattice

Superlattice	$\delta E_{\rm rel}$	$\delta E^{\rm int}_{\rm rel}/\delta E_{\rm rel}$	$\lvert\delta E_{\rm rel}/\Delta H(A_2B_2)\rvert$
Ni_2Au_2	-216.5	0.88	3.08
Cu_2Au_2	-143.1	0.84	21.36
Cu_2Ag_2	-96.7	0.90	1.24
Ni_2Al_2	-303.9	0.50	0.69
Cu_2Al_2	-88.2	0.80	1.19
Al_2Mg_2	-34.6	1.00	2.52

A_1B_1 (001) Superlattice

Superlattice	$\delta E_{\rm rel}$	$\delta E^{\rm int}_{\rm rel}/\delta E_{\rm rel}$	$\lvert\delta E_{\rm rel}/\Delta H(A_1B_1)\rvert$
Ni_1Au_1	-22.0	0.0	0.29
Cu_1Au_1	-12.1	0.0	0.25
Cu_1Ag_1	-7.1	0.0	0.07
Ni_1Al_1	-141.7	0.0	0.21
Cu_1Al_1	-115.9	0.0	0.71
Al_1Mg_1	$\sim$0	-	$\sim$0

FIGURES

FIG. 1. Schematic illustration of the classification of alloy types in terms of energies of ordered (O) compounds, random (R) alloys, and coherent phase separation, or coherency strain (CS) minimized with respect to orientation. Note that the energy difference O→R and O→CS give the ordering energy and the coherent phase separation energy, $\delta E_{\rm ord}$ and $\delta E_{\rm CPS}$, respectively. Energies are shown relative to the reference state of incoherent phase separation (IPS) $A + B$, labelled as "0.0" to indicate the zero of energy. The ordered structures "O" are meant to be representative of the lowest-energy structures with dominant composition waves at the Brillouin zone boundary (e.g., the $L1_0$, $L1_1$, or $L1_2$ structures). It should be noted that in cases (e.g., Al-Cu) where the lowest-energy coherent configurations correspond to ordered compounds which have a large degree of "clustering", one can obtain clustering-type SRO even in a "Type I" alloy (see Ref. [14]).

FIG. 2. Energetics of Cu_4Au_1 (210) superlattice relative to Cu_3Au ($L1_2$) and Cu.

FIG. 3. The calculated and measured [30] SRO patterns $\alpha(\mathbf{k})$ in $Cu_{0.90}Au_{0.10}$. Shown are the calculated results for both (a) non-attenuated coherency strain, (b) attenuated coherency strain, and (c) the experimentally measured pattern extracted from diffuse x-ray scattering. SRO is shown in the $(hk0)$ plane, and peak contours are shaded black.

FIG. 4. The calculated SRO patterns $\alpha(\mathbf{k})$ in $Al_{0.85}Mg_{0.15}$. SRO is shown in the $(hk0)$ plane, and peak contours are shaded black.

FIG. 5. The calculated SRO patterns $\alpha(\mathbf{k})$ in $Ga_{0.50}In_{0.50}P$. SRO is shown in the $(hk0)$ plane, and peak contours are shaded black.

FIG. 6. The calculated SRO patterns $\alpha(\mathbf{k})$ in $Ni_{0.75}Au_{0.25}$. Shown are the calculated results for both (a) non-attenuated coherency strain and (b) attenuated coherency strain. SRO is shown in the $(hk0)$ plane, and peak contours are shaded black.

FIG. 7. The calculated SRO patterns $\alpha(\mathbf{k})$ in $Ni_{0.40}Au_{0.60}$. Shown are the calculated results for both (a) non-attenuated coherency strain and (b) attenuated coherency strain. SRO is shown in the $(hk0)$ plane, and peak contours are shaded black.

FIG. 8. The calculated SRO pattern $\alpha(\mathbf{k})$ in $Cu_{0.95}Ag_{0.05}$. SRO is shown in the $(hk0)$ plane, and peak contours are shaded black.

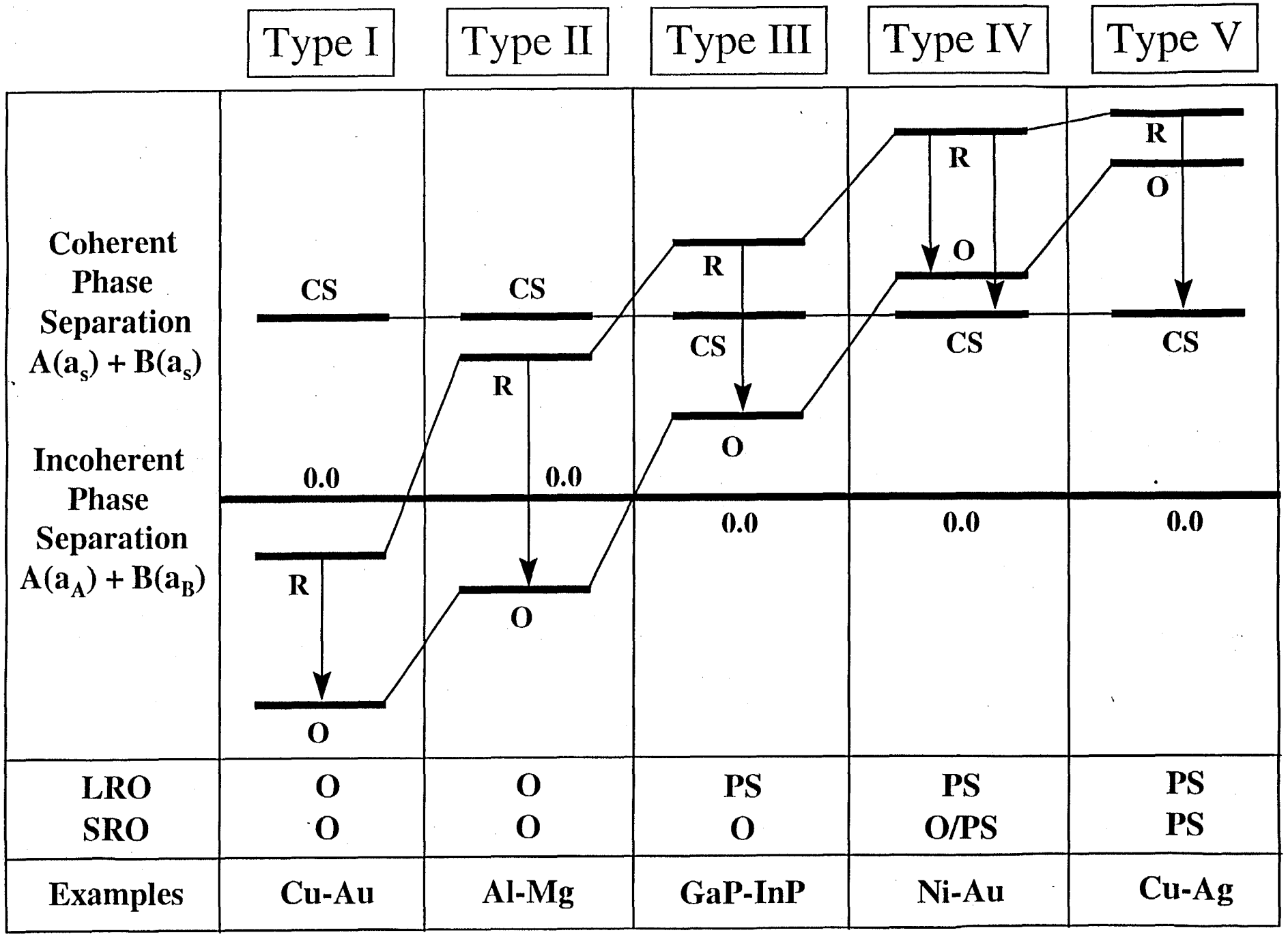
Type I
Type II
Type III
Type IV
Type V
Coherent Phase Separation $A(a_s) + B(a_s)$
Incoherent Phase Separation $A(a_A) + B(a_B)$
CS
R
O
0.0
LRO
SRO
Examples
O
O
Cu-Au
O
O
Al-Mg
PS
O
GaP-InP
PS
O/PS
Ni-Au
PS
PS
Cu-Ag

Fig. 1

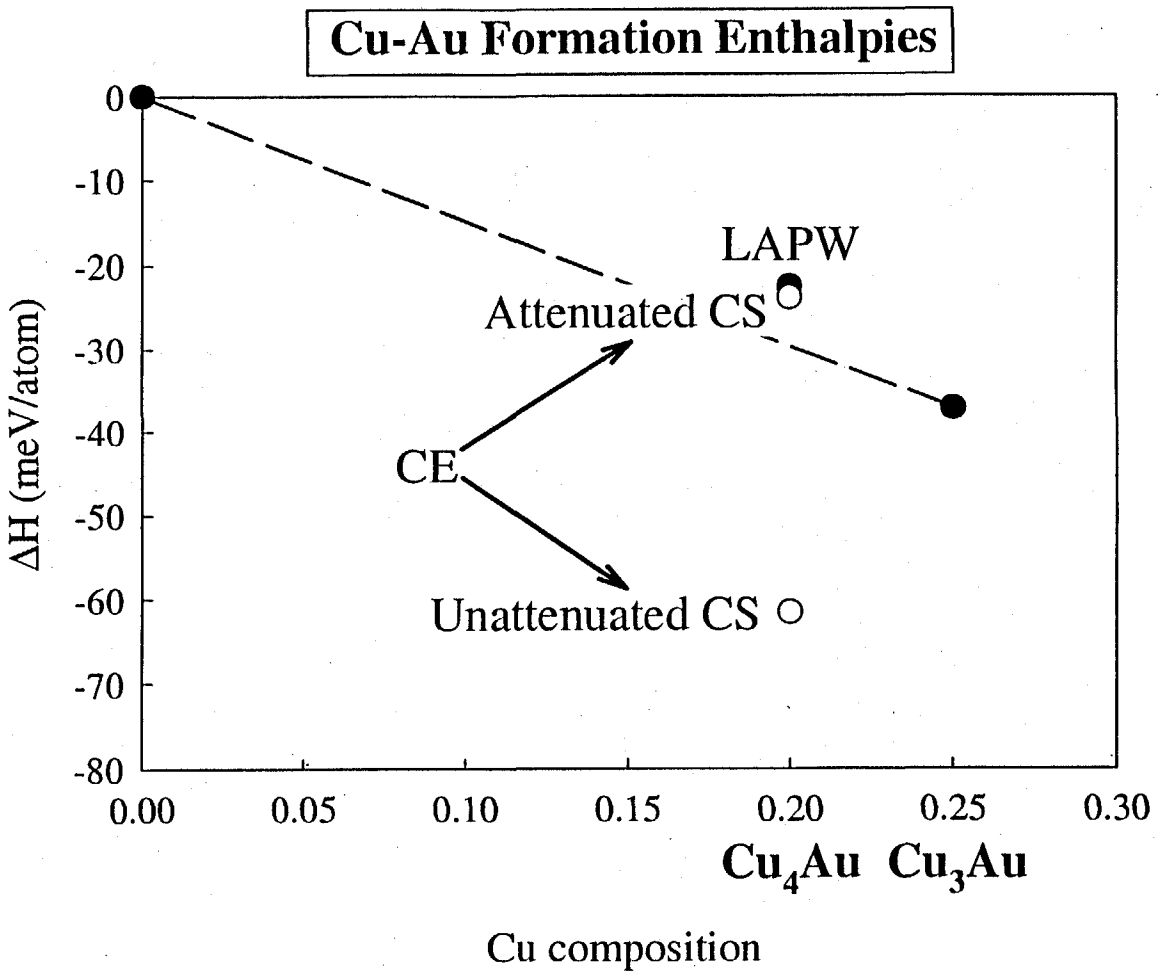
Cu-Au Formation Enthalpies
0
-10
-20
-30
-40
-50
-60
-70
-80
ΔH (meV/atom)
LAPW
Attenuated CS
CE
Unattenuated CS
0.00
0.05
0.10
0.15
0.20
0.25
0.30
Cu4Au
Cu3Au
Cu composition

Fig. 2

Short-Range Order of $Cu_{0.9}Au_{0.1}$

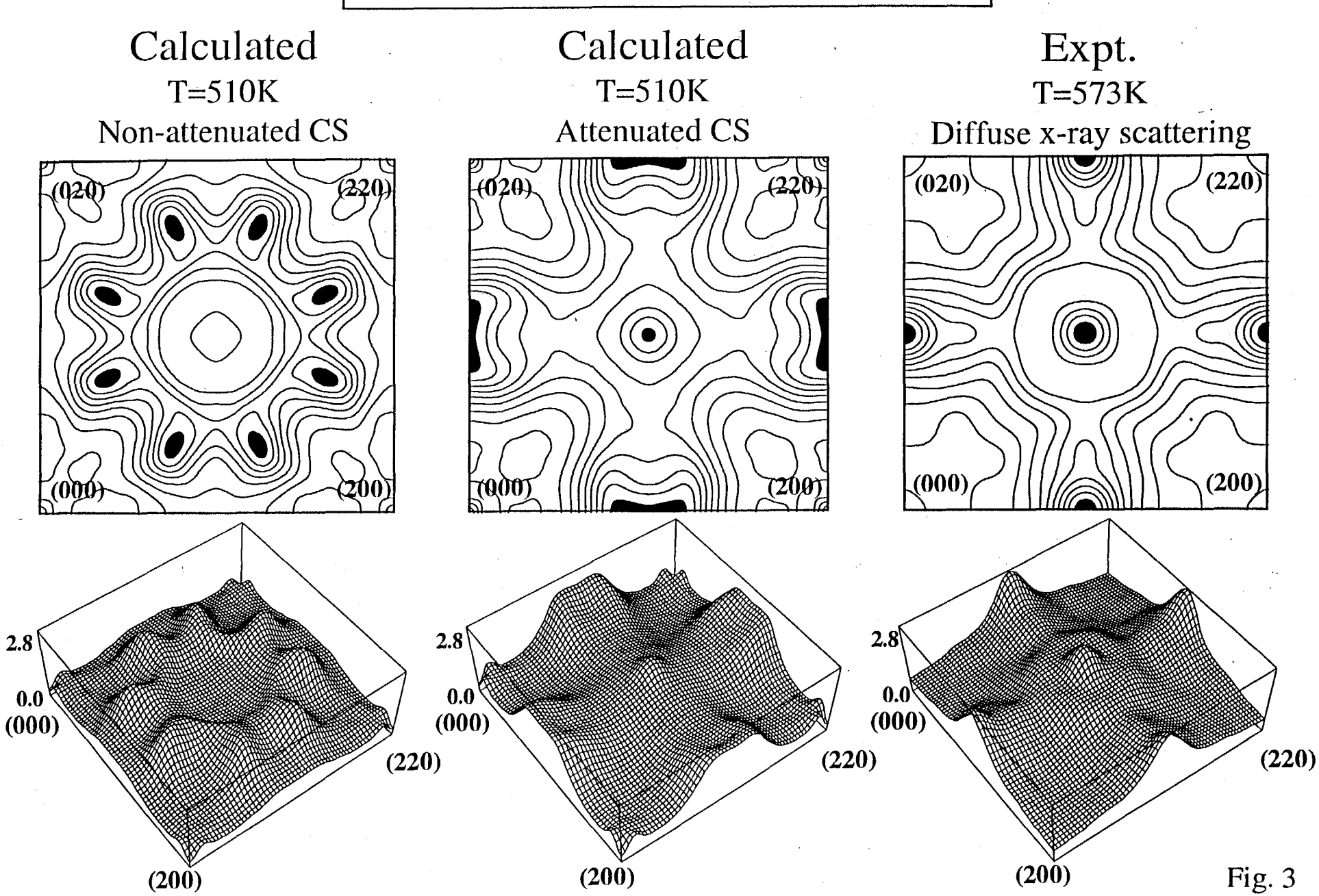

Fig. 3

Short-Range Order of $Al_{0.85}Mg_{0.15}$

T=350K

Attenuated CS

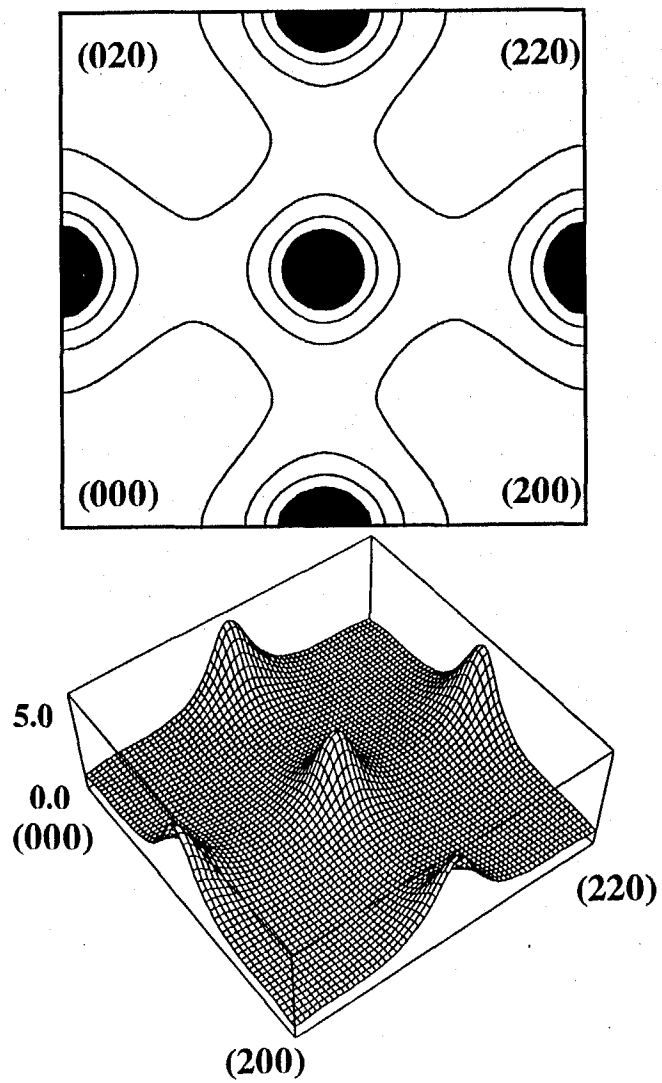

Fig. 4

Short-Range Order of $Ga_{0.5}In_{0.5}P$

Calculated
T=1000K
Non-attenuated CS

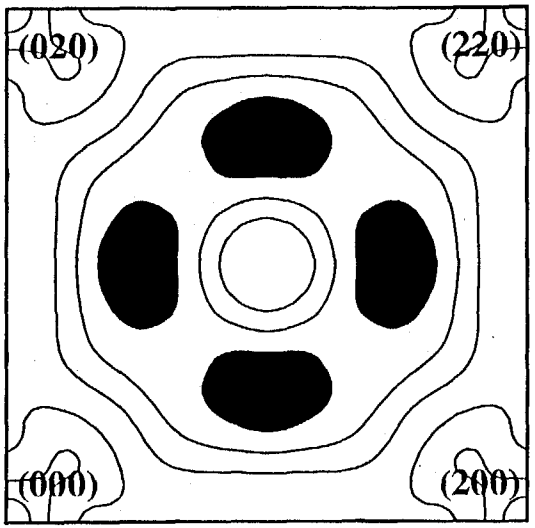

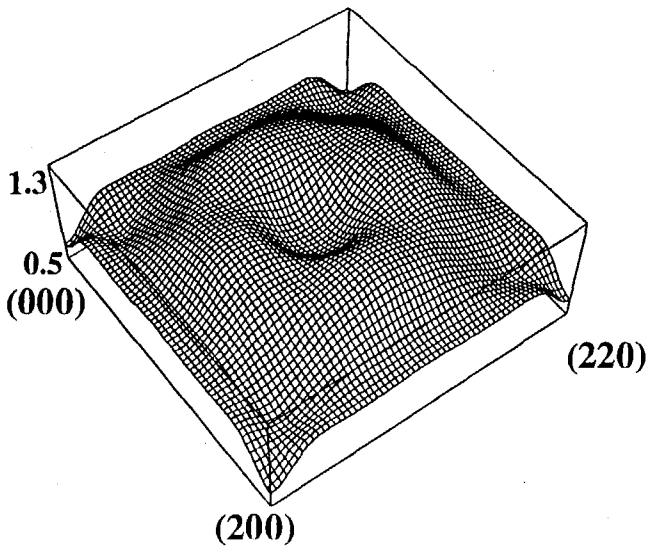

Calculated
T=250K
Non-attenuated CS

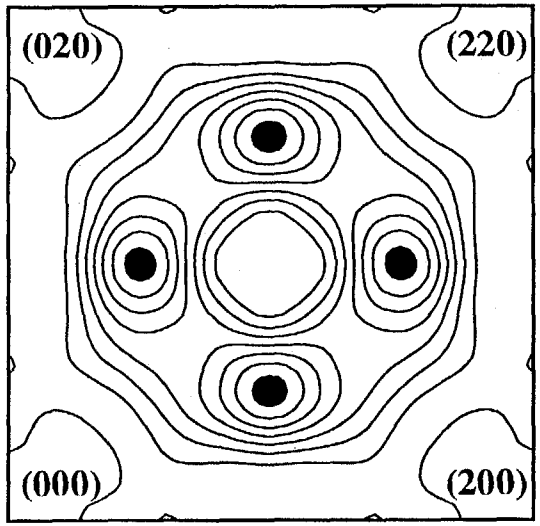

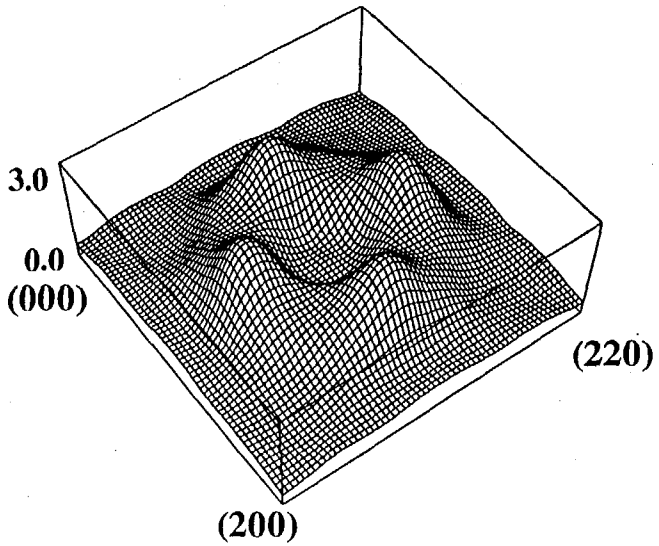

Fig. 5

Short-Range Order of $Ni_{0.75}Au_{0.25}$

Calculated
T=2300K
Non-attenuated CS

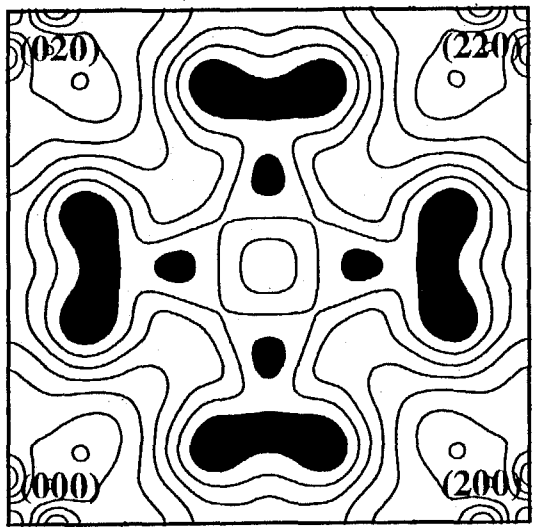

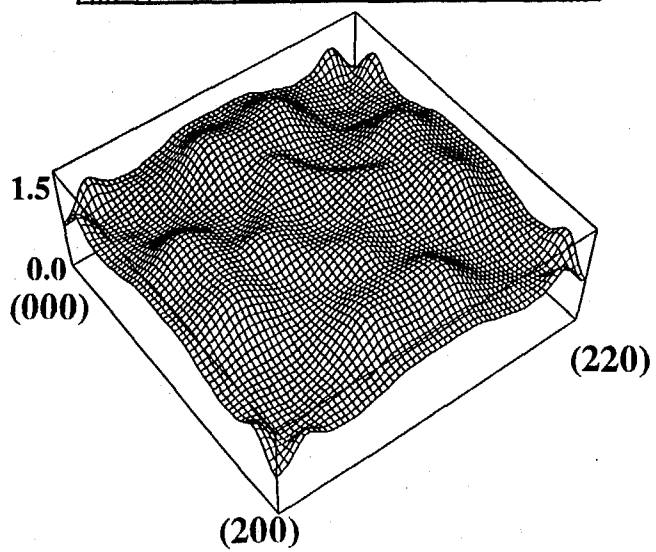

Calculated
T=2300K
Attenuated CS

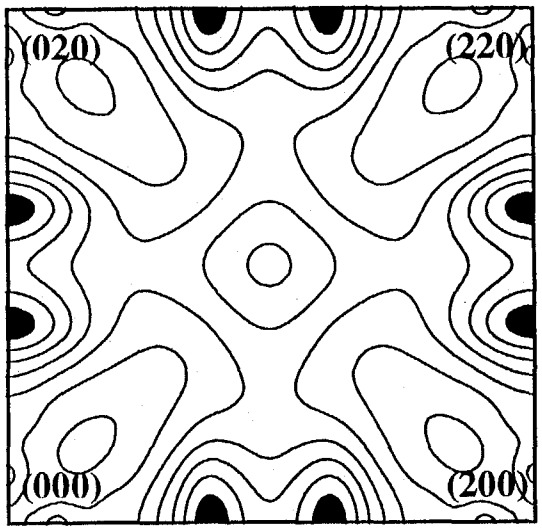

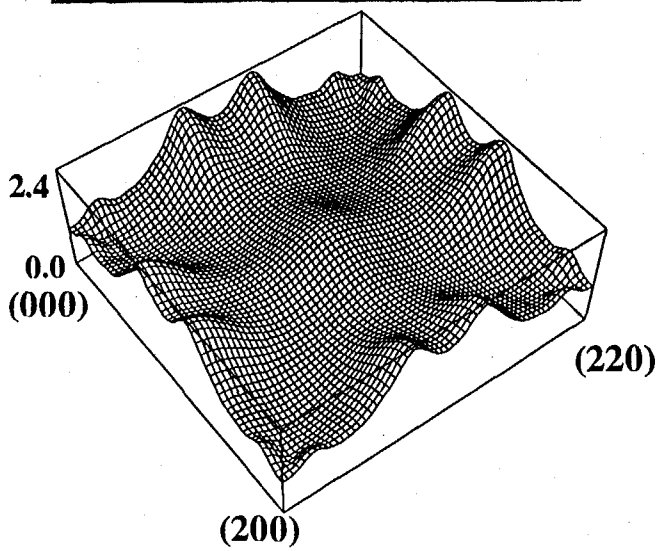

Fig. 6

Short-Range Order of $Ni_{0.4}Au_{0.6}$

Calculated
T=2300K
Non-attenuated CS

Calculated
T=2300K
Attenuated CS

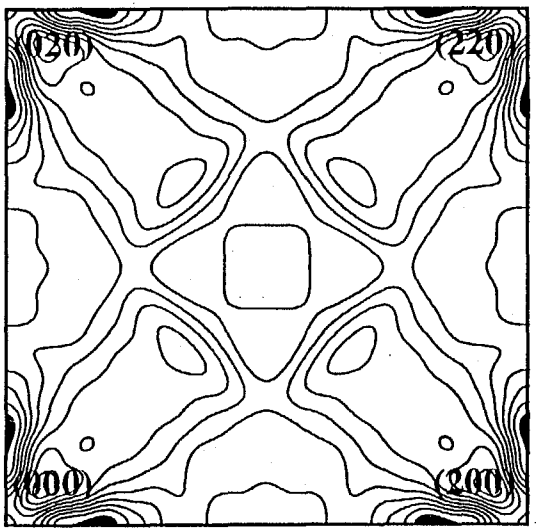

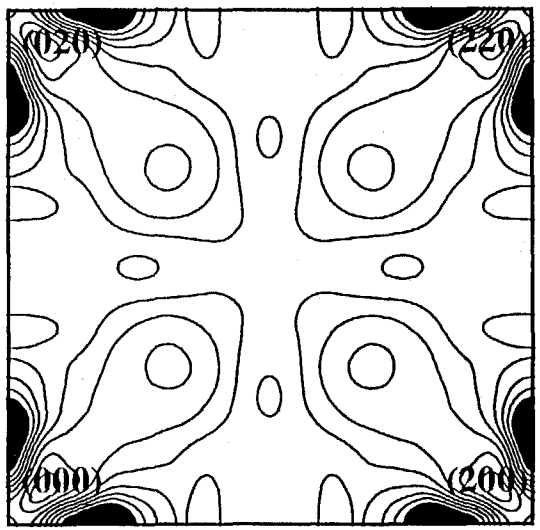

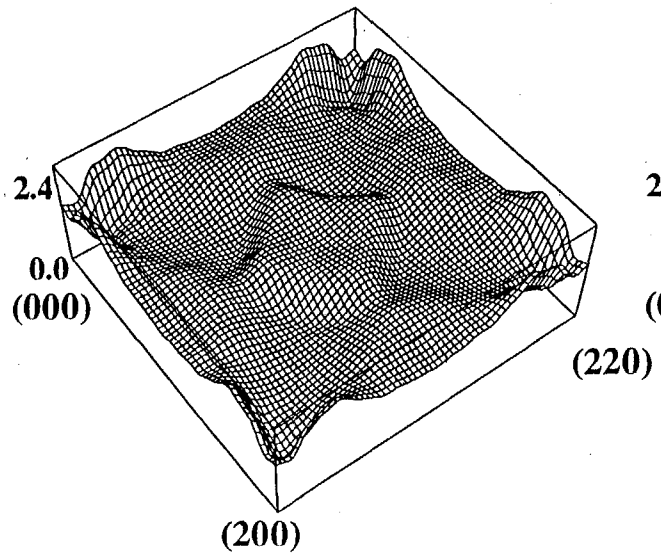

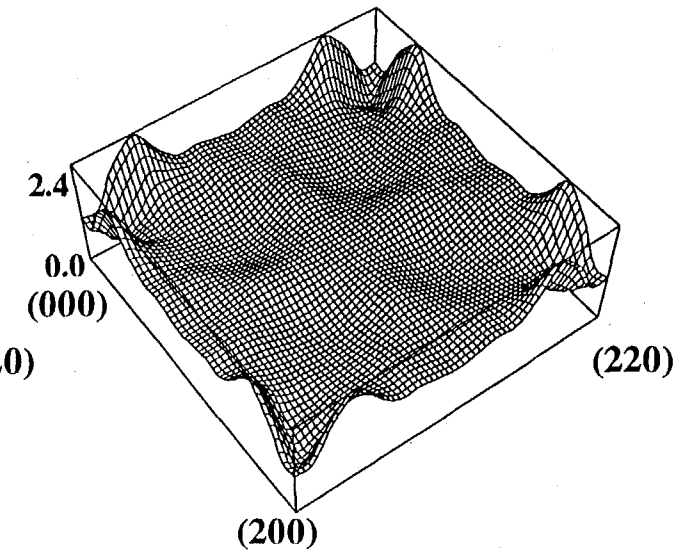

Fig. 7

Short-Range Order of $Cu_{0.95}Ag_{0.05}$

T=480K

Non-attenuated CS

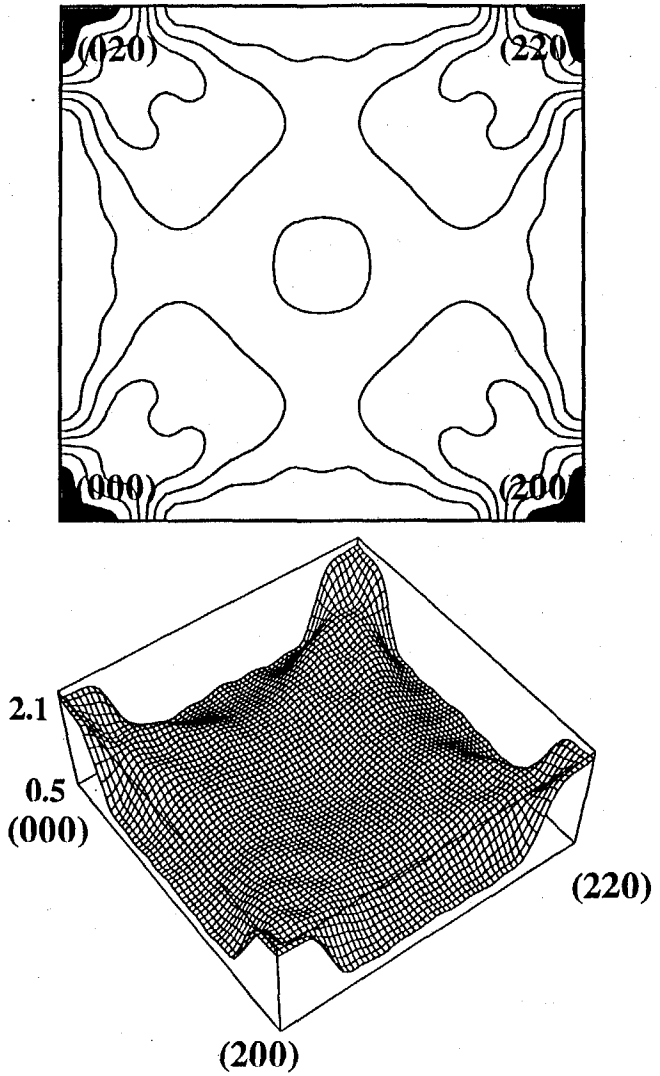

Fig. 8